JOURNAL OF GEOPHYSICAL RESEARCH, VOL. 107, NO. D8, 10.1029/2001JD001216, 2002

Jicamarca radar observations of the diurnal and semidiurnal tide in the troposphere and lower stratosphere

Dennis M. Riggin,[1] Erhan Kudeki,[2] Zhaomei Feng,[2] Martin F. Sarango,[3] and Ruth S. Lieberman[1]

Received 22 July 2000; revised 13 February 2001; accepted 9 August 2001; published 23 April 2002.

[1] The mesosphere-stratosphere-troposphere (MST) radar at Jicamarca, Peru (12°S, 77°W), made extended (15 day or longer) observations of the horizontal and vertical winds that were used to infer the diurnal and semidiurnal tides. The measurements were made during several months from mid-1997 through mid-1998 and using a higher-power transmitter and finer range resolution during 10 days of August 1998. The three-component winds are used to estimate amplitudes, phases, and momentum fluxes associated with the tides. Thermal forcing of the diurnal tide is also examined with diurnal water vapor heating rates calculated using data from the NASA Water Vapor Project (NVAP). For the region near Jicamarca the calculations from NVAP showed the temporal variability of the diurnal heating to be dominated by an annual cycle with maximum around the summer solstice. When projected into tidal modes, about 25% of the total water vapor heating rate amplitude near Jicamarca is found to be nonmigrating. The meridional amplitude of the semidiurnal tide was found to be generally greater than the zonal amplitude, although tidal theory predicts that the zonal amplitude should be much greater at the latitude of Jicamarca (assuming the tide was migrating). The phase of the semidiurnal tide lagged (by about 3 hours) the phase expected from surface pressure climatologies. According to tidal theory the migrating semidiurnal tide should transport little meridional momentum flux. However, substantial southward fluxes ($\langle v'w' \rangle \sim -1 \times 10^{-3}$ m^2 s^{-2}) were observed at Jicamarca, and the meridional component of momentum flux was typically larger in magnitude than the zonal component was. The diurnal tide was somewhat weaker, was less coherent, and transported less momentum. The semidiurnal tide had a very long vertical wavelength throughout the troposphere and into the lower stratosphere, while the diurnal tide was only observed to propagate at heights above the tropopause with a much shorter (~10 km) vertical wavelength. Below the tropopause the dominant diurnal motions were not traveling waves, but rather convective motions that exhibited little phase progression with altitude. These motions were broadly peaked in frequency around 24 hours and were presumably standing oscillations with no horizontal propagation and probably with small horizontal scale. Despite the lack of coherence of these quasi-diurnal motions, the associated vertical wind amplitudes were sizable (~0.02 m s^{-1}), and thus the fluctuations can presumably transport significant horizontal momentum. *INDEX TERMS:* 3384 Meteorology and Atmospheric Dynamics: Waves and tides; 3374 Meteorology and Atmospheric Dynamics: Tropical meteorology; 3314 Meteorology and Atmospheric Dynamics: Convective processes; 3309 Meteorology and Atmospheric Dynamics: Climatology (1620); *KEYWORDS:* tide, troposphere, stratosphere, momentum flux, radar

1. Introduction

[2] This paper reports momentum fluxes and other observed characteristics associated with the diurnal and semidiurnal tides. The observations were made with the Jicamarca radar in Peru from mid-1997 through mid-1998. The radar observations allow direct measurement of the horizontal and vertical wind fluctuations and momentum fluxes. We will also briefly discuss the tidal forcing near Jicamarca, making use of the NASA Water Vapor Project (NVAP) data set to infer the annual variation in the diurnal heating rate.

[1]Colorado Research Associates Division, NorthWest Research Associates, Inc., Boulder, Colorado, USA.
[2]Department of Electrical and Computer Engineering, University of Illinois, Urbana, Illinois, USA.
[3]Instituto Geofisico del Perú, Jicamarca Radio Observatory, Lima, Peru.

Copyright 2002 by the American Geophysical Union.
0148-0227/02/2001JD001216$09.00

[3] Tidal modes may be categorized as either migrating or nonmigrating. The term "migrating" refers to that component of the tide that propagates westward with a phase speed synchronized with the apparent motion of the Sun. Many characteristics of the migrating tides can be deduced from classical tidal theory. Assuming a 260 K isothermal atmosphere, the gravest symmetric, migrating semidiurnal tide theoretically has a 311 km vertical wavelength, compared with the 28 km vertical wavelength of the gravest symmetric, migrating diurnal tide [*Forbes*, 1995]. Below 30 km the percentage of nonmigrating components in the semidiurnal tide has been reported as small compared with the percentage of nonmigrating components in the diurnal tide [*Wallace and Tadd*, 1974]. This preponderance of migrating components is confirmed by the tall linear structure of the semidiurnal tide and the shorter, more complicated structure of the diurnal tide along the equator in European Centre for Medium-Range Weather Forecasts (ECMWF) analyses [*Hsu and Hoskins*, 1989].

[4] Figure 1 shows theoretically predicted Hough mode wind structures for the migrating diurnal and semidiurnal wind tides,

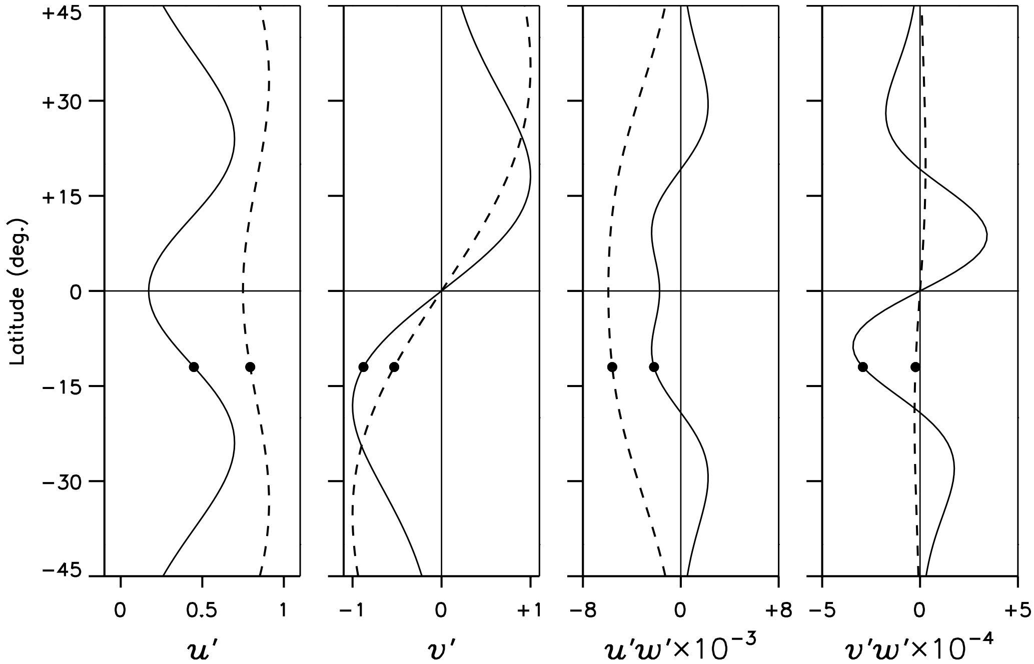

Figure 1. Hough mode migrating tidal structures for *u* and *v* and estimates of *uw* and *vw* found from continuity. The solid (dashed) curves pertain to the diurnal (semidiurnal) tide. The solid circles denote the latitude of Jicamarca.

assuming a windless isothermal atmosphere. The zonal (u') and meridional (v') components of the wind are in phase quadrature and rotate anticyclonically with respect to time and height in each hemisphere. The v' components vanish at the equator, but increase rapidly with latitude away from this node. At the 12°S latitude of Jicamarca, the magnitude of v' is approximately twice that of u' for the diurnal tide, while the horizontal wind components of the semidiurnal tide are of comparable amplitude at this latitude. The continuity relation allows the divergence of the vertical tidal wind (w') to be calculated from the divergence of the horizontal winds [*Lindzen*, 1990]. It is possible, in turn, to estimate w', assuming a height dependence of exp $[1/(2H) - im]z$, where H is the scale height and m is the vertical wave number. For this rough calculation we assumed $H = 6$ km and vertical wavelegths of 28 km (311 km) for the diurnal (semidiurnal) tides. The right-hand panels of Figure 1 show the momentum flux components derived from the horizontal and vertical wind components. Classical tidal theory gives no information regarding wave amplitudes. However, horizontal wind amplitudes for the tides on the order of 1 m s^{-1} are observed in the troposphere/lower stratosphere. The maximum horizontal wind in Figure 1 has been normalized to this value. Thus the $u'w'$ and $v'w'$ values shown in Figure 1 should roughly correspond to actual tidal momentum fluxes in the troposphere/lower stratosphere in units of m^2 s^{-2}, assuming that the migrating components dominate. The migrating tides transport mostly westward momentum at low latitudes. For $m = 0$, w is phase with u'. Thus the migrating semidiurnal tide, which is known to have an extremely long vertical wavelength (small m) should transport negligible meridional momentum flux. For the diurnal tide, $v'w'$ is divergent (i.e., poleward) at low latitudes. At the latitude of Jicamarca the migrating diurnal tide should have a zonal momentum flux ~7 times greater in magnitude than the meridional momentum flux.

2. Tidal Excitation

[5] Although the propagation of the tides is well described by a classical theory, the excitation of the diurnal tide involves more uncertain factors, such as atmospheric composition and atmospheric turbulence [e.g., *Chapman and Lindzen*, 1970]. The dominant excitation mechanism for the diurnal tide in the lower atmosphere is the direct absorption of sunlight by water vapor (sensible heating). This heating process is the main source of the migrating diurnal tide. Figure 2 shows the diurnal heating rate amplitude averaged over a slab extending from 700 to 300 hPa (~3–9 km), where most of the water vapor heating occurs.

[6] The heating rate was computed from monthly mean grids of total precipitable water (TPW) from the NASA Water Vapor Project (NVAP) data set [*Randal et al.*, 1996]. Global TPW was inverted to form vertical profiles of tropospheric specific humidity on a global 1° × 1° latitude-longitude grid. Vertical profiles

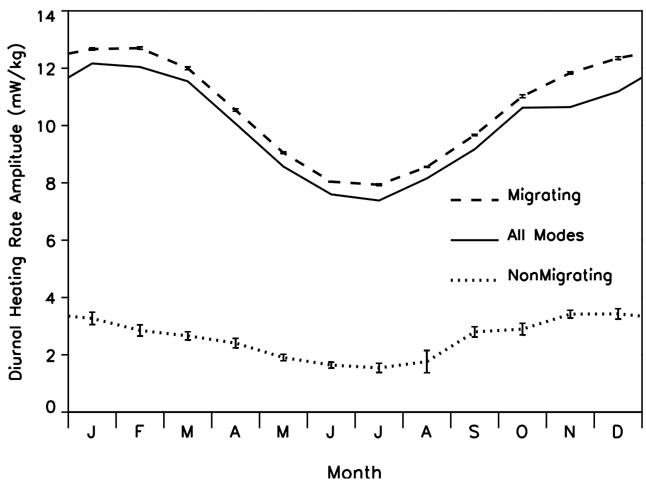

Figure 2. Diurnal water vapor heating rate amplitudes calculated from satellite data for a point located near Jicamarca (12.5°S, 80°W). The heating rate is composited over 5 years of observation and is averaged over a slab extending from 700 to 300 hPa.

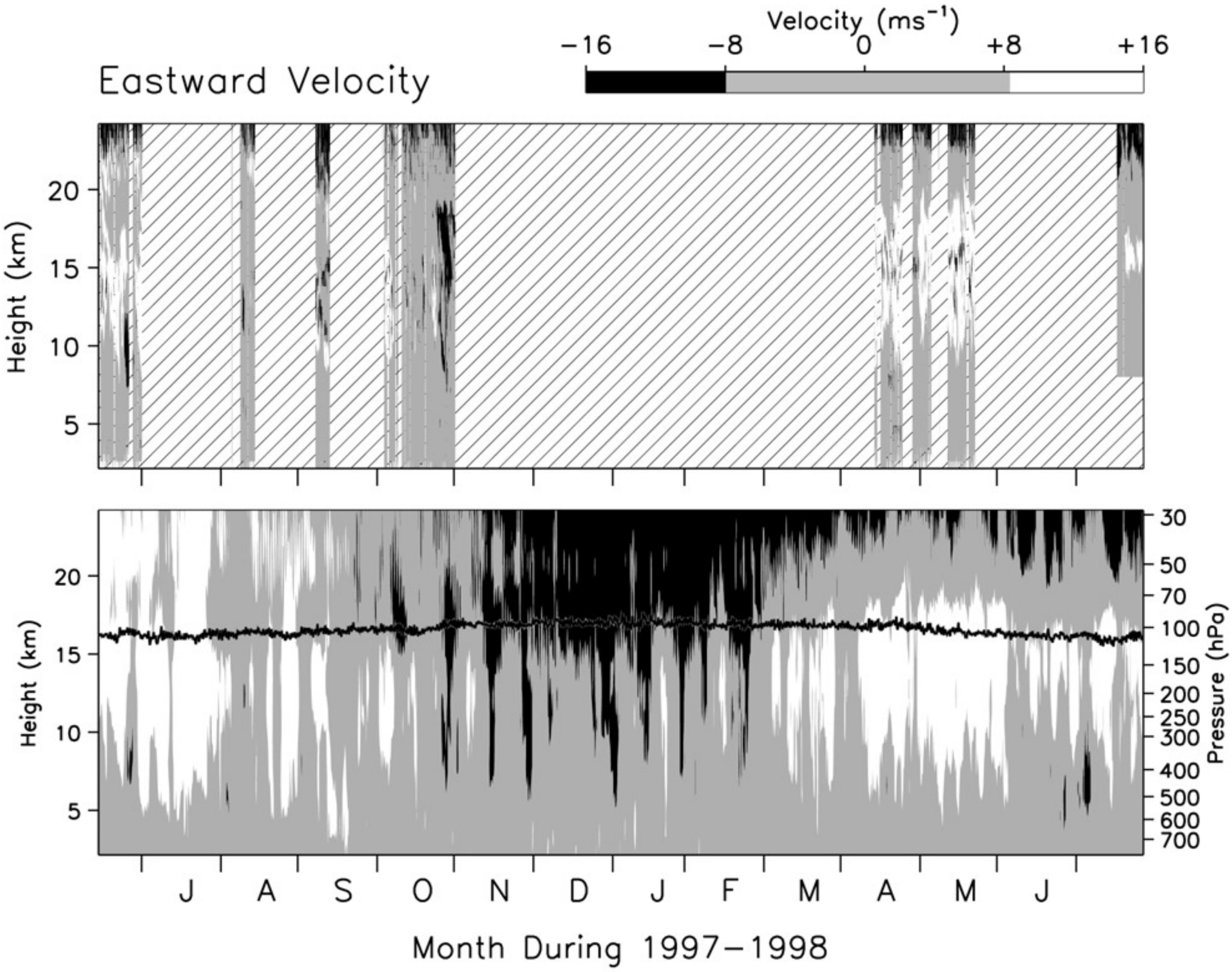

Figure 3. Eastward wind (top) obtained with Jicamarca radar and (bottom) from 6 hour NCEP-NCAR reanalysis. The thick black curve (bottom panel) shows the height of the tropopause. See color version of this figure at back of this issue.

of diurnal heating rates were then computed at each grid point on a 1.5° × 2.5° latitude-longitude grid using the model of *Groves* [1982] with the climatological cloud data of *Warren et al.* [1986, 1988]. Figure 2 was generated from NVAP TPW spanning 1988–1992. The 2.5° longitudinal resolution allows the heating rate to be decomposed into zonal wave number. The solid curve in the figure shows the sum of all zonal wave numbers out to wave number ±35, the dotted curve shows the nonmigrating component, and the dashed curve shows the migrating component. Although the nonmigrating heating is ~25% of the total heating, the total heating rate amplitude (nonmigrating plus migrating) is actually slightly less than that contributed by the migrating component alone. The nonmigrating modes tend to be out of phase with the migrating component and partially cancel the diurnal heating cycle. Long-term temporal variability in water vapor heating is dominated by an annual cycle with a ~40% drop in both the migrating and total heating rates from summer solstice to winter solstice. In Figure 2 the error bars on the migrating and nonmigrating curves show the scatter in the monthly heating rate estimates as $\pm\sigma/\sqrt{n}$, where $n = 5$ and σ is the standard deviation of the estimates over the 5 years. The error bars are almost indistinguishable for the migrating component because there was little variation between corresponding months over the 5 years.

[7] Another leading contributor to diurnal tidal excitation in the tropics is latent heat release associated with convection. This source is enhanced over land mass areas and appears to contribute to the larger diurnal tide amplitudes over the continents as compared to the oceans [*Hamilton*, 1981]. Other more uncertain contributors to tidal excitation include topographic irregularities in surface heating that are coupled to the atmosphere by turbulent processes and land-sea contrast (e.g., sea breeze flowing over orography) [*Kato*, 1980]. The tropospheric sources other than water vapor heating tend to be localized, contributing mainly a nonmigrating component to the forcing. The amplitudes of the diurnal tidal winds in the tropical lower stratosphere (~24 km) vary considerably with season, more so than the amplitudes in the lower troposphere [*Wallace and Tadd*, 1974]. Owing to its high zonal phase speed, the migrating diurnal tide should propagate into the stratosphere with relative insensitivity to the prevailing winds. Thus the seasonal variability of the diurnal tide in the lower stratosphere may be partly caused by filtering of the more slowly propagating nonmigrating modes. Above 200 hPa (~26 km), *Wallace and Tadd* [1974] found that localized features became muted and the diurnal tidal wind structure became global in scale. The dominant driving mechanism for the migrating semidiurnal tide is ozone absorption in the upper stratosphere and lower mesosphere. The semidiurnal tide excited at these heights is

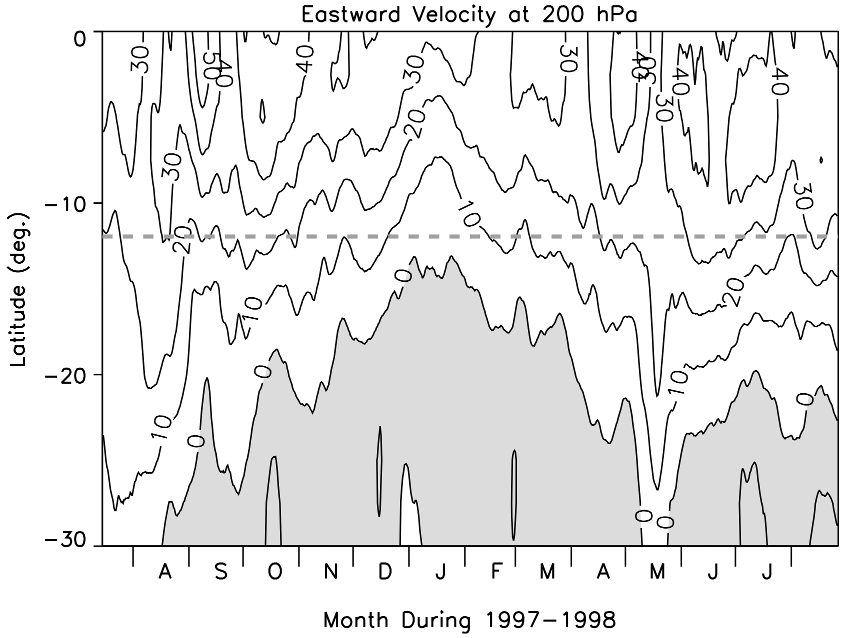

Figure 4. Eastward wind at the 200 hPa level taken from 6 hour NCEP-NCAR reanalysis and smoothed with a 15 day running mean. The dashed grey line shows the latitude of Jicamarca, and westward winds are shaded.

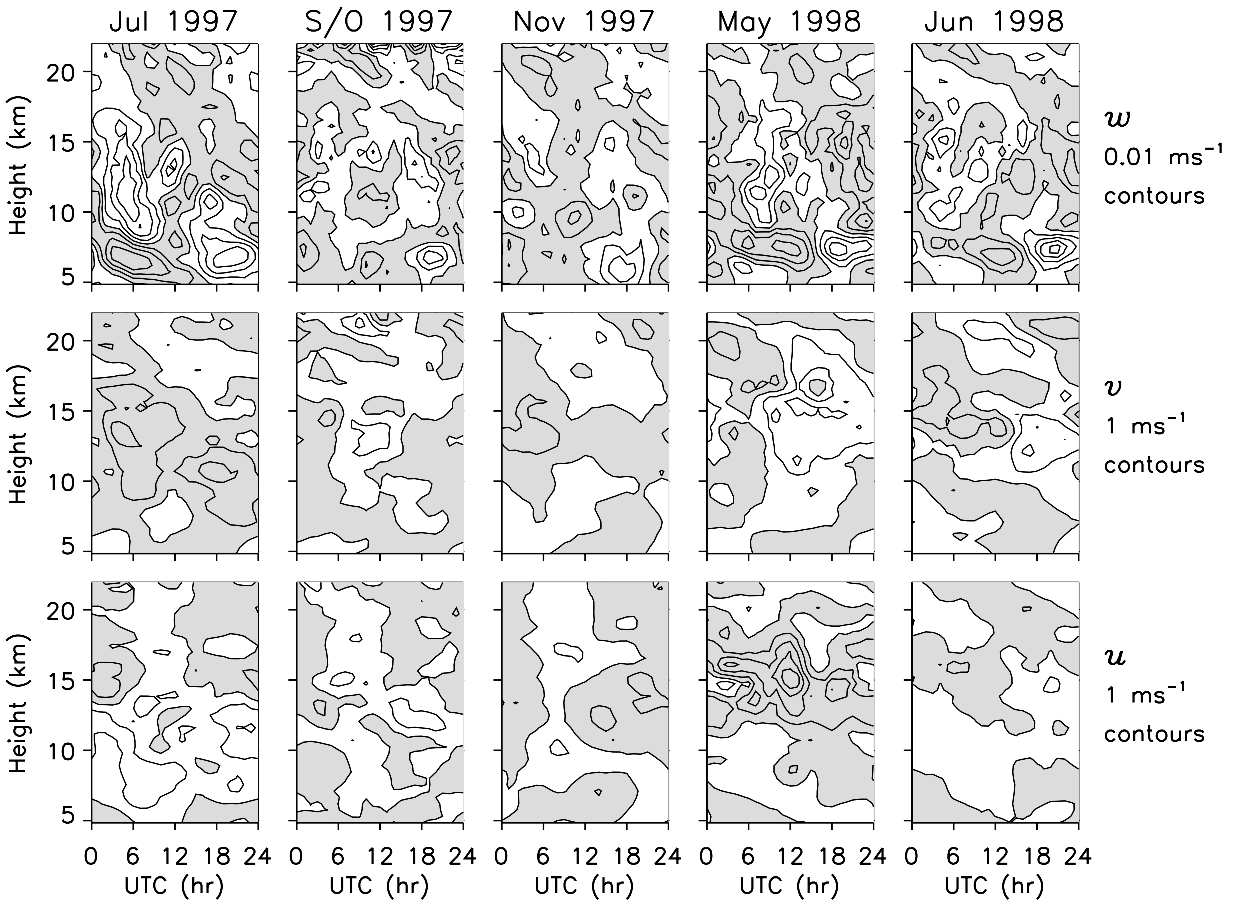

Figure 5. Daily composites of *u*, *v*, and *w* fields for the month indicated. The "S/O 1997" label refers to composites for September–October 1997. Shading corresponds to negative values.

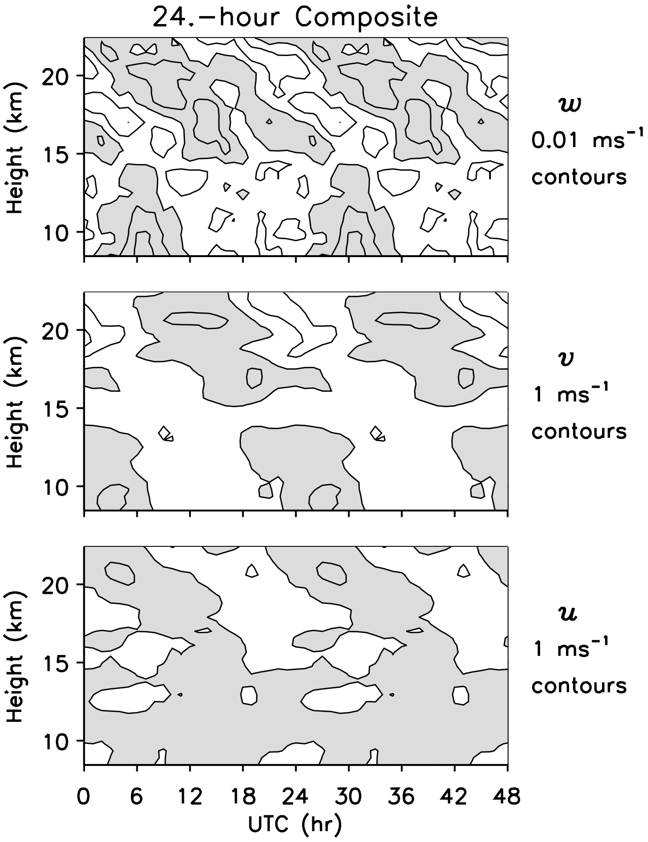

Figure 6. Diurnal tidal composites of high-passed *u*, *v*, and *w* fields from the August 1998 10-day campaign. Shading corresponds to negative values. Two cycles of the tide are shown.

predominantly a migrating mode that propagates all the way to the surface [*Kato*, 1980].

3. Jicamarca Radar Data Collection and Analysis Methodology

[8] The Jicamarca Radio Observatory (11.95°S, 76.87°W) is located on a low coastal plain near Lima, Peru, between the Pacific coast and Andes Cordillera. The Intertropical Convergence Zone is located ∼5°–10°N, well to the north of Jicamarca, and the region has little rainfall. However, although a desert, coastal Peru is often blanketed with fog. Most of the mesosphere-stratosphere-troposphere (MST) observations made at Jicamarca have been subject to interruption during the nighttime hours, so the diurnal tide has been previously little studied at this site. The Jicamarca Long-Term Investigation of the Ionosphere and Atmosphere (JULIA) system consists of two 30 kW power transmitters connected to the large Jicamarca array which can run unattended and hence collect data over extended periods. Between July 1997 and June 1998 the radar collected numerous days of wind measurements in the JULIA mode with at least 15 days of observation for five individual monthly or bimonthly periods. In JULIA mode the radar measured Doppler wind velocities from ∼3 to 22 km with good (1.36 min) time resolution, but relatively coarse (1 km) range resolution. In addition, 10 days of nearly continuous measurements were made in August 1998. During this run the 2 MW transmitter peak power was used during the day, and two 100 kW transmitters were used during the nighttime hours. The radar pulses were coded with a 16 baud complementary code with a baud width corresponding to 450 m resolution, and usable winds were collected over heights of ∼8 to 23 km with 1 min time resolution. The experiment configuration was similar to earlier 10 day campaigns at Jicamarca [e.g., *Riggin et al.*, 1997], except that measurements were continued during the nighttime hours. For the measurements presented in this paper, the antenna was divided into four quadrants with each of the four beams pointing 2.5° off vertical toward the north, south, east, and west. The small zenith angle is necessary to avoid sidelobes but is probably nearly ideal for measuring vertical velocities. Biases due to specular reflection from layers are minimized because the half-width, two-way, half-power beam widths in the beam tilt direction are only ∼0.6°. Details on the processing used to obtain line-of-sight velocities from the raw data are given by *Hitchman et al.* [1997].

4. Jicamarca Radar Results

[9] Figure 3 provides an overview of the eastward winds obtained with the Jicamarca radar during 1997–1998. The lower panel shows 6 hour National Centers for Environmental Prediction—National Center for Atmospheric Research (NCEP-NCAR) reanalysis [*Kalnay et al.*, 1996] eastward winds for the same period. The pressure labels on the right-hand axis show the heights at which reanalysis winds are reported. The black curve in the reanalysis panel shows the tropopause. Above the tropopause, westward shear in the mean winds persisted from October 1997 onward. During July–August 1997 and during April–July 1998 an eastward jet was centered in the upper troposphere at 200 hPa. However, as shown by Figure 4, this wind pattern was interrupted by the northward intrusion of midlatitude westward winds during the middle months (centered around January of 1998), nearly reaching the latitude of Jicamarca.

[10] Although only intermittent radar observations were made, several months have sufficient data to make tidal composites of winds. Diurnal composites prepared from the JULIA data for July 1997, September–October 1997 (two months combined), November 1997, May 1998, and June 1998 are shown in Figure 5. The composites were compiled by binning each component of the wind into hourly bins, high-pass filtering the winds with a band edge of 36 hours, averaging corresponding times over the multiple days of data, and subtracting any residual mean. Each composite shown in Figure 5 contains 15–27 days of data. There is considerable month-to-month persistence in the tidal structures of Figure 5, particularly at heights above the tropopause. Figure 6 shows similar tidal composites from the August 1998 10-day campaign. In Figure 6 the v' component lags u', so the horizontal wind vector is rotating in the anticyclonic direction with increasing time. This is the direction of rotation usually observed in the Southern Hemisphere [e.g., *Hsu and Hoskins*, 1989] and expected from gravity wave theory. The phase relationships between u' and v' are not clear in Figure 5.

[11] Useful quantities, such as the amplitudes, phases, and momentum fluxes associated with the tides, can be computed from the composites shown in Figures 5 and 6. Amplitudes of the diurnal and semidiurnal tide obtained by singular value decomposition (SVD) fitting are shown in Figure 7. On average, the semidiurnal tide has a larger amplitude than the diurnal tide, although the semidiurnal tide exhibits deep amplitude minima. The amplitude minima could correspond to destructive interference between different modes. However, the vertical wavelength of the interfering modes would have to be quite short to explain the vertical separation of the amplitude minima. In the case of the semidiurnal tide (but not the diurnal tide) the superimposed modes are likely to include a migrating component propagating downward from the stratosphere. However, note that the diurnal and semidiurnal tides do not always appear as independent modes. On occasion (e.g., the u' profiles for June 1998) the diurnal and semidiurnal tidal amplitude profiles are highly correlated. Correlated amplitude peaks such as these may correspond to convective motions. The phases corresponding to the amplitudes in Figure 7

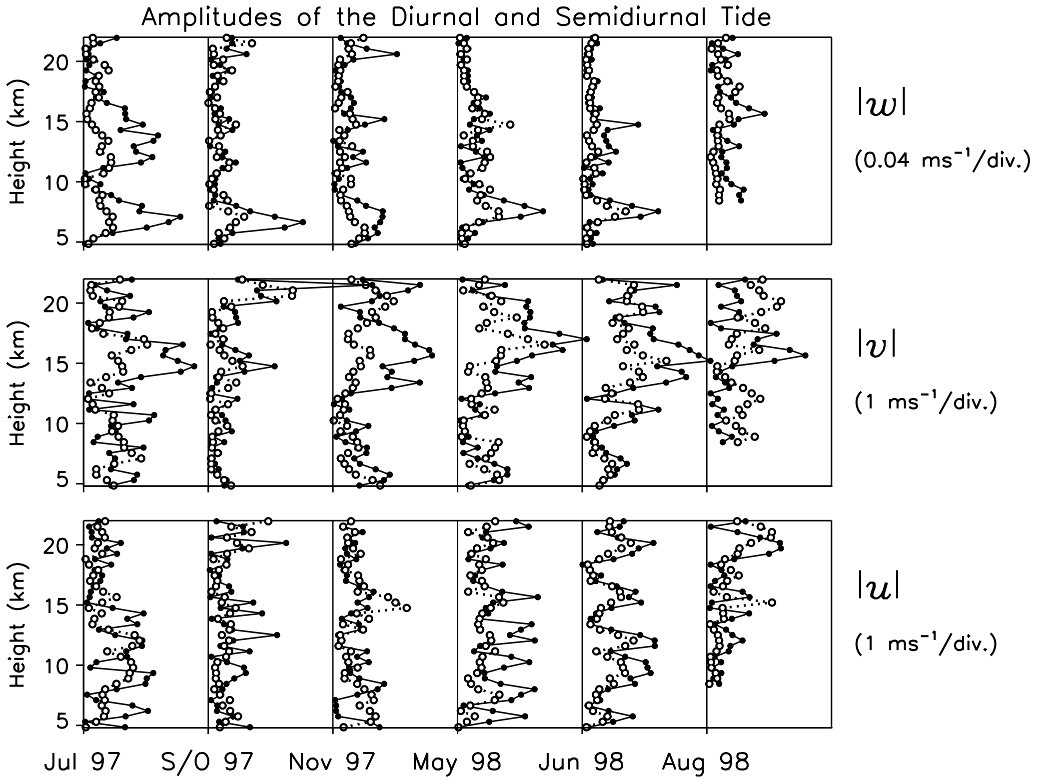

Figure 7. Amplitude profiles of the diurnal tide (open circles, dashed curves) and the semidiurnal tide (solid circles, solid curves). Annotations on the right-hand side show the component (vertical, meridional, or zonal) and the velocity offset between profiles. The "S/O 1997" label refers to composites for September–October 1997.

are shown in Figure 8. The phases are not always coherent, but some general features can be discerned. The diurnal phases are nearly vertical below the tropopause and then exhibit a decreasing phase progression with height with a vertical wavelength of ~10 km. The semidiurnal phases show only a slight decrease with height and lack the sudden change in behavior at the tropopause that characterizes the diurnal phases. The semidiurnal phases are not inconsistent with the 331 km vertical wavelength derived from theory for the migrating (gravest symmetric) semidiurnal tide (assuming a 256 K isothermal atmosphere [*Forbes*, 1995]). The gravity wave polarization relations provide a means of crudely estimating the horizontal wavelength of the diurnal tide by multiplying the vertical wavelength by the ratio of horizontal to vertical wind amplitudes. Assuming a 10 km vertical wavelength and diurnal horizontal and vertical wind amplitudes of $\sim$1 m s^{-1} and $\sim$0.004 m s^{-1}, respectively (see Figure 7), yields a horizontal wavelength of 2500 km. Such a mesoscale tide should be well described by linear (f plane) gravity wave theory [*Lindzen*, 1970]. Our estimate of horizontal wavelength only applies to the diurnal tide at heights above the tropopause. At lower heights, localized convective motions augment the diurnal vertical amplitudes.

[12] The composites can also be used to compute momentum fluxes associated with the tide by simply multiplying the horizontal and vertical composited fields similar to those shown in Figures 5 and 6 and then summing over a wave period. The vertical tidal composites displayed in these figures combine data from all four beams, but only vertical velocities from coplanar beams were used for computing the vertical fluxes of eastward and northward momentum. Using only coplanar information prevents $u'v'$ products from leaking into the estimates of the vertical flux of horizontal momentum. Another complication in estimating momentum fluxes is that the 24 hour composites shown in Figures 5–6 contain both a semidiurnal as well as a diurnal tide. In fact, the composites will contain all even submultiples of the diurnal tide. However, we expect tidal harmonics higher than terdiurnal to be negligible, and odd harmonics like the terdiurnal tide cancel when making the diurnal composite. Therefore, to calculate fluxes, we generated semidiurnal composite fields (not shown) and then subtracted these composite fields from the corresponding 24 hour composites to yield a relatively pure diurnal composite. The fluxes were computed ateach height and then averaged into 4 km bins. After the 4 km height averaging, the semidiurnal momentum fluxes shown in Table 1 are typically greater than those of the diurnal tide. Although some of the vertical wind amplitudes shown in Figure 7 appear to be unrealistically large for a migrating semidiurnal tide, these vertical winds were partly associated with convective motions. The 4 km vertical averaging suppresses the effect of incoherent vertical motions that do not maintain a constant phase relationship with the horizontal motions as a function of height. The momentum fluxes shown in Table 1 are typically southward ($\langle v'w' \rangle \sim -1 \times 10^{-3}$ m^2 s^{-2}), and typical horizontal wind amplitudes associated with the semidiurnal tide can be found from Figure 7 ($v' \sim 0.3$ m s^{-1}). The semidiurnal vertical wind amplitude implied by the ratio of momentum flux to the horizontal wind amplitude is 3×10^{-3} m s^{-1}. The semidiurnal momentum fluxes were consistently southward until the August 1998 campaign, when they reversed sign and became northward. The zonal momentum fluxes are weaker and show less consistency. The actual effective fluxes are somewhat reduced by the multiplicative factor $(1-f^2/\hat{\omega}2)$. This correction is due to the meridional heat flux associated with the wave perturbations [*Fritts and Vincent*, 1987]. We have not applied this correction to the flux values in Table 1, because the intrinsic tidal frequencies ($\hat{\omega}$) are not known to high accuracy. Making a crude assumption that $\hat{\omega}$ roughly corresponds to the extrinsic 24 hour period, the correction is 0.81 for the diurnal tide and 0.95 for the semidiurnal tide.

[13] We now examine the character of the tidal motions in greater detail, focusing on the 10 day August 1998 campaign.

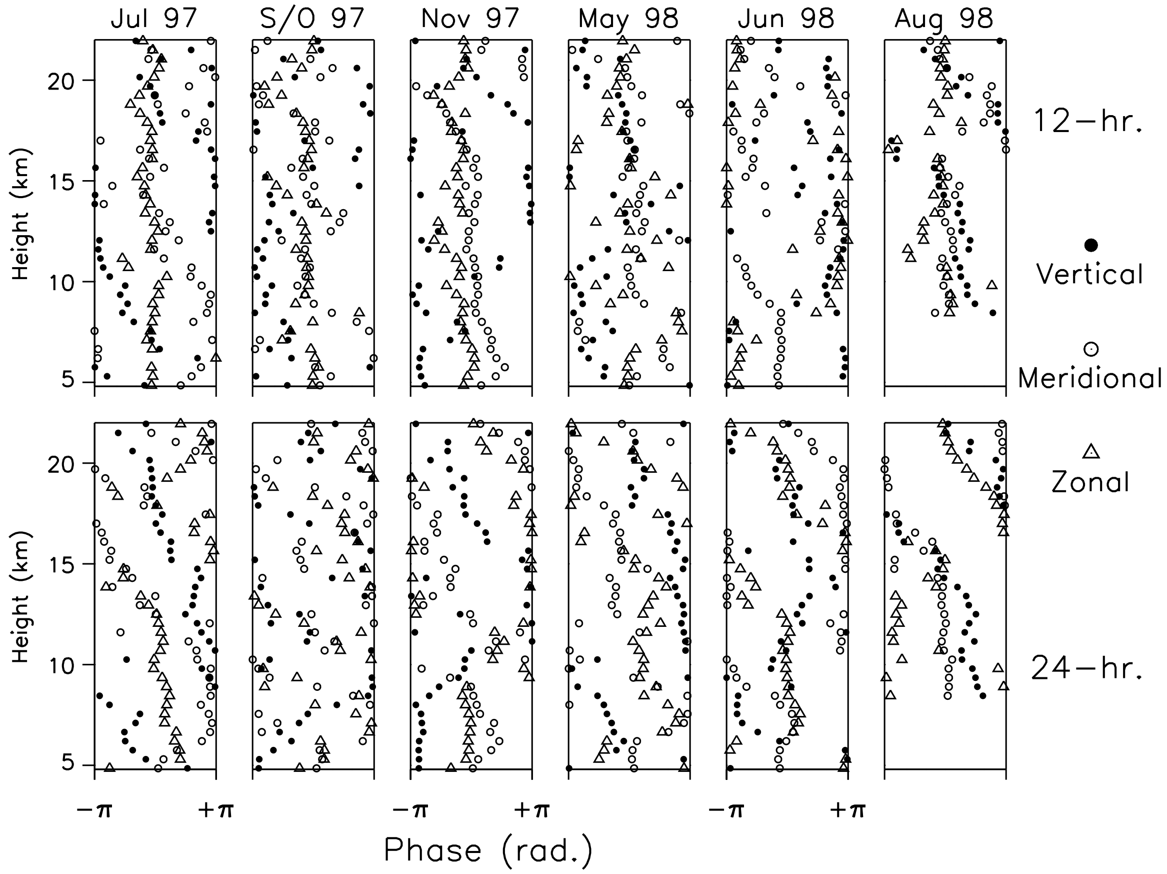

Figure 8. Phase of the (top) semidiurnal tide and (bottom) diurnal tide. The phase angle extrema of ±π correspond to ±12 hours in the case of the diurnal tide and ±6 hours in the case of the semidiurnal tide. The symbols are plotted at the time of positive maximum in each of the wind components (eastward, northward, and vertical). The "S/O 1997" label refers to composites for September–October 1997.

Power spectra of the horizontal and vertical wind fluctuations are shown in Figure 9. The spectra were smoothed with a running mean boxcar average with the number of points in the smoothing window increasing with the square root of frequency. The grey diagonal bars show slopes corresponding to $f^{-5/3}$ and the grey vertical lines show decades above the 2 min Nyquist period.

[14] The spectra above the 16 km tropopause show distinct peaks at the buoyancy period (~5 min). The power spectral density produced by a 2×10^{-2} m s^{-1} test signal is shown in the first panel. The power spectral density of the test signal relative to the data gives an indication of the radar sensitivity. The buoyancy fluctations are clearly above the noise level and are at a similar value of power spectral density. At frequencies higher than the buoyancy frequency, the vertical velocity power spectra fall off precipitously. However, data gaps were linearly interpolated when generating the power spectra, and this suppresses the high frequencies in the spectra to some degree. Since buoyancy waves are not seen at lower levels, their excitation may be associated with the higher static stability above the tropopause. At all heights the spectra also show peaks at periods of ~24 hours in the horizontal and vertical winds. A 12 hour peak is also evident in some of the spectra, particularly in the vertical wind spectra for 12.05–15.65 km.

[15] Below the tropopause (8.00–15.65 km) the horizontal component power spectral density (PSD) peaks in Figure 9 are separated from the vertical component peaks by only ~1000, corresponding to a ratio of ~30 in velocity. The frequency dependence of the horizontal velocity spectra is consistent with the $f^{-5/3}$ gravity wave spectrum (compare grey diagonal bars) [*VanZandt*, 1985] only at low frequencies and becomes whiter than the −5/3 slope at higher frequencies. The vertical spectra are nearly as steep as the horizontal wind spectra, much steeper than the $f^{-1/3}$ canonical slope [*Fritts and VanZandt*, 1987]. Doppler shifting does not explain the redness of the vertical wind spectra because the mean wind was weak. Instead, we suggest that the vertical wind fluctuations were dominated by convective motions rather than gravity waves. Figure 10 shows these vertical convective motions clearly. The winds in this figure were high-pass Hanning filtered in the time domain with

Table 1. Eastward and Northward Tidal Momentum Fluxes Averaged Over 4 km Intervals[a]

	6–10 km		10–14 km		14–18 km		18–22 km	
Time	$u'w'$	$v'w'$	$u'w'$	$v'w'$	$u'w'$	$v'w'$	$u'w'$	$v'w'$
July 1997	−0.7	−2.1	0.1	−2.1	−0.7	−0.8	−0.3	−0.4
	(0.3)	(−0.1)	(0.2)	(0.4)	(0.1)	(0.4)	(0.1)	(−0.1)
S/O 1997	0.2	0.1	−0.1	−1.2	0.1	−1.2	0.7	−2.9
	(0.3)	(−0.1)	(0.0)	(−0.2)	(0.0)	(−0.2)	(0.1)	(0.4)
Nov. 1997	−0.3	−1.2	−0.2	−0.2	0.1	−0.9	−0.7	−0.9
	(0.1)	(−0.1)	(−0.3)	(0.2)	(0.2)	(0.1)	(0.0)	(−0.1)
May 1998	−0.3	−0.9	−0.2	−0.6	0.1	−1.7	−0.7	−1.1
	(0.1)	(−0.1)	(0.5)	(−0.5)	(0.3)	(0.0)	(0.0)	(−0.1)
June 1998	−2.5	−1.2	0.7	−1.0	−1.3	−1.5	0.0	−1.2
	(0.0)	(−0.1)	(0.3)	(−0.3)	(0.0)	(−0.2)	(0.0)	(−0.1)
Aug. 1998	0.2	1.0	−0.3	0.5	1.0	1.6	0.6	0.6
	(−0.2)	(−0.1)	(−0.3)	(0.0)	(0.2)	(0.0)	(0.0)	(0.3)

[a]Fluxes are given in units of m^2 s^{-2} × 10^{-3}. Semidiurnal fluxes are given in the upper row for each monthly period and diurnal fluxes are given in the lower row in parentheses. The "S/O 1997" label refers to composites for September–October 1997.

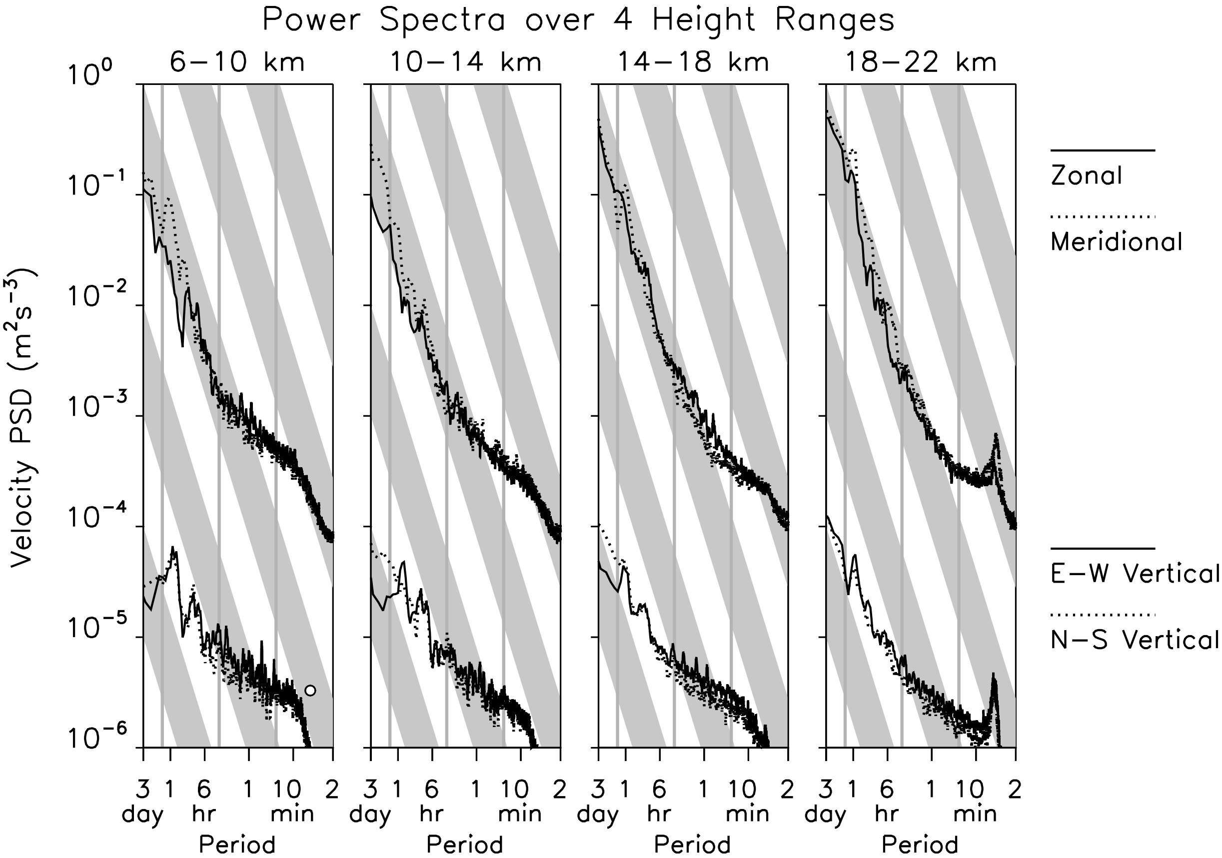

Figure 9. Power spectra of the zonal (solid curves) and meridional (dashed curves) winds from the 10 day August 1998 campaign. On the same scale are shown power spectra of vertical winds estimated from the sum of the east/west beams (solid curves) and north/south beams (dotted curves). Power spectra are averaged over nine heights and then smoothed with a running boxcar proportional to $f^{1/2}$. Grey vertical lines show decades above the 2 min Nyquist frequency. Grey diagonal bars show a slope corresponding to a $-5/3$ power law. The white circle in the first panel is a spectral peak at a period of 5 min corresponding to a 2×10^{-2} m s^{-1} test signal.

a half-amplitude band edge at 36 hours (the same filter as used for Figure 6).

[16] Below the tropopause there is no vertical phase variation in the motions, although there is a quasi-tidal periodicity. The alternating updrafts and downdrafts in the vertical wind component presumably correspond to convective motions with small horizontal scales. Coherent wave activity was mostly absent in the troposphere, although a wave with ~8 hour period is visible at lower altitudes in the *u* component during 22–23 August (see Figure 10a).

5. Discussion

[17] We have found the semidiurnal tide to be persistent motion in the troposphere and lower stratosphere over Jicamarca. The diurnal tide is somewhat weaker, is less coherent, and transports much less momentum. The semidiurnal tide had a long vertical wavelength throughout the troposphere and into the lower stratosphere. The diurnal tide was only observed to propagate above the tropopause with a vertical wavelength of ~10 km. Below the tropopause the dominant motions were not waves, but rather convective motions that exhibited little phase progression with altitude. These motions were broadly peaked in frequency around 24 hours and were presumably standing oscillations with no horizontal propagation and small horizontal scale. Despite the lack of coherence of these quasi-diurnal motions, the associated vertical wind amplitudes were sizable (~0.02 m s^{-1}), and thus can presumably transport significant horizontal momentum. Diurnal tidal phases, derived by sinusoidal fits to the winds, have a complicated and irregular vertical structure in the troposphere. The apparent irregular vertical structure reflects the incoherence of the motions in this region but is also affected by the poor quality of the fits where the tidal amplitude is weak. The propagating tide may be excited near the tropopause, with the strong vertical convective motions in the troposphere (as seen in Figure 10) as a source of excitation. Although this is a possible scenario, there is inherent ambiguity in data from a single location. For example, the tidal motions we observed at Jicamarca below the tropopause could be mostly regional in scale, while the motions above the tropopause contained a higher proportion of larger-scale tides not directly associated with the tidal motions observed below.

[18] Our current understanding of the tide in the troposphere and lower stratosphere is based to large degree on inferences from satellite measurements and models. Over the continental landmasses the forcing due to latent heat release (inferred from satellite-observed cloud top temperatures) is strongly enhanced around the diurnal period [*Salby and Garcia*, 1987; *Bergman and Salby*, 1994]. On the basis of model results, *Sassi and Garcia* [1997] have argued that quasi-diurnal period tidal motions are crucial sources of westward momentum for the tropical semiannual oscillation (SAO) at the stratopause and mesopause. Most of the direct observations of the diurnal tide in the tropical lower stratosphere have been made by radiosonde. However, inertia-gravity waves are often the dominant horizontal motions in the tropical lower stratosphere and can make the tide difficult to observe. Separating the tide from inertia-gravity waves often requires compositing and ~10 or more nearly contin-

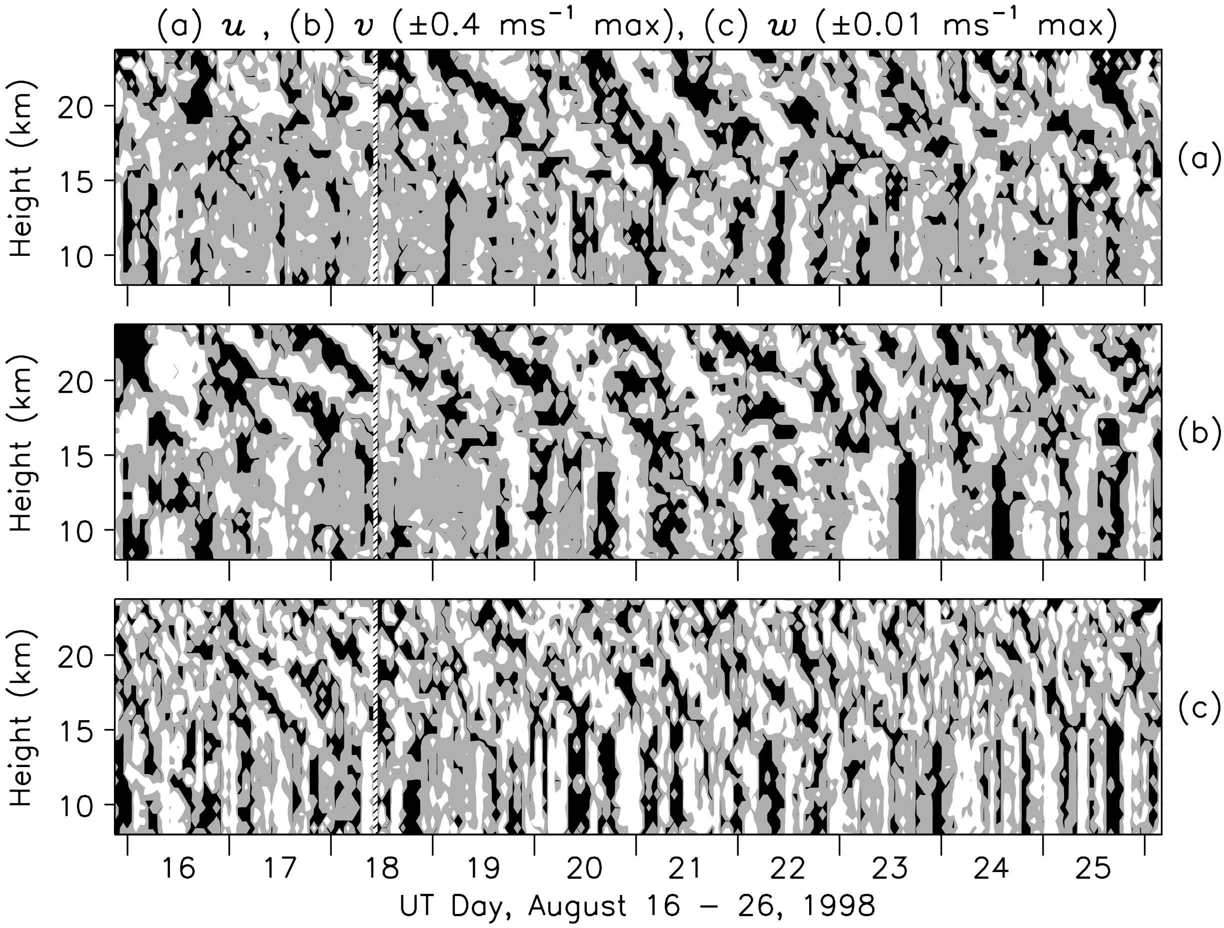

Figure 10. Hourly averaged (a) zonal wind, (b) meridional wind, and (c) vertical wind are shown high-pass filtered with a 36 hour band edge. The three-level grey scale saturates at ±0.4 ms^{-1} for the horizontal wind components and ±0.01 ms^{-1} for the vertical. Wind values below the negative saturation level (values above the positive saturation level) are denoted by black (white).

uous days of observations. Prior to 1997, MST measurements at Jicamarca were seldom extended to nighttime hours, making tidal observations impossible. *Fukao et al.* [1978] were the first to observe the diurnal tide at Jicamarca. Although this was only a single day of observation, the horizontal and vertical wind amplitudes of the diurnal tide were quite similar to those we observed. Similar horizontal wind amplitudes of the diurnal tide have been observed with radiosonde from western Pacific sites [*Tsuda et al.*, 1995, 1997] and with tropical Pacific wind profilers [*Williams and Avery*, 1996]. On the basis of a 4 year composite of tidal winds from a wind profiler in the equatorial Pacific, *Williams et al.* [1992] concluded that the diurnal and semidiurnal tides were predominantly migrating. The phases and amplitudes of the diurnal tides were reported to undergo relatively little seasonal variation in the troposphere [*Williams and Avery*, 1996]. In contrast, the tides we observed at Jicamarca appear to have been predominantly nomigrating, regional-scale waves.

[19] There are few radiosonde observations of the semidiurnal tide in the tropical troposphere and lower stratosphere, because the data records often lack sufficient time resolution. *Williams et al.* [1992] concluded that the semidiurnal tide observed by wind profiler near the equator was migrating, based on the consistency of the observed winds with a climatology of surface pressure. The 12 hour pressure, derived from harmonic analysis of global surface data (presumed to be the migrating mode), peaks at local mean solar times of 0936 and 2136 LMST [*Haurwitz and Cowley*, 1973]. These times should correspond to the westward semidiurnal wind maximum for the dominant (migrating) mode (see Figure 1 of *Whiteman and Bian* [1996]). At Jicamarca (see Figure 8) we found a zonal (eastward) wind maximum near 0000 UT at low altitudes. The corresponding westward wind maxima were at ~0600 and 1800 UT, which correspond to ~0100 and 1300 LMST. This phase does not agree closely with the *Haurwitz and Cowley* [1973] global surface climatology. Our semidiurnal winds were also inconsistent with the Hough mode solution for the migrating semidiurnal tide. The semidiurnal tidal momentum flux was typically southward over Jicamarca with a typical value of $\langle v'w' \rangle \sim -1 \times 10^{-3}$ m^2 s^{-2}. This flux is much bigger in magnitude than that predicted from tidal theory for the migrating component (see Figure 1). The tidal equations yield a meridional wind amplitude for the migrating semidiurnal tide that is much weaker than the zonal for the latitude of Jicamarca (12°S), but we found the meridional amplitudes to be as large or larger (see Figure 7).

[20] The semidiurnal tidal momentum flux was typically southward over Jicamarca ($\langle v'w' \rangle \sim -1 \times 10^{-3}$ m^2 s^{-2}). To put this value in context with other stratospheric momentum flux estimates, the $\langle u'w' \rangle$ transported by Kelvin waves (as estimated indirectly from radiosonde w' and T' fields) is ~2–8 × 10^{-3} m^2 s^{-2} [*Wallace and Kousky*, 1968; *Maruyama*, 1994]. Rossby-gravity waves contribute a westward (negative) $\langle u'w' \rangle$ with a magnitude roughly half that contributed by the Kelvin waves [*Dunkerton*, 1997]. *Sasi et al.* [1999] directly measured substantially larger magnitudes of $\langle u'w' \rangle$ with the Indian MST radar at Gadanki, India (13.5°N, 79.2°E). However, these $\langle u'w' \rangle$ estimates used w computed from beams that were not all coplanar. Use of noncoplanar beams could mix $\langle u'w' \rangle$ products in with the desired vertical fluxes of horizontal momentum.

[21] The strongest El Niño event on record occurred during the years 1997–1998 [*McPhaden*, 1999], and thus the tidal data presented in this paper may not reflect the normal climatology of the region. *Sato and Dunkerton* [1997] have presented evidence that coherent inertia-gravity waves are suppressed when the quasi-biennial oscillation (QBO) mean zonal wind shear is westward. The lower stratospheric wind shear was in fact westward over Jicamarca for the mid-1997 to mid-1998 period (see Figure 3) discussed in this paper. In fact, the inertia-gravity waves do appear to have been less prevalent than during earlier campaigns at Jicamarca [*Riggin et al.*, 1995, 1997]. Inertia-gravity waves have amplitudes that are comparable to or somewhat larger than the tides, but they have much shorter (3–5 km) observed vertical wavelengths in the tropics [*Riggin et al.*, 1995, 1997; *Tsuda et al.*, 1994; *Shimizu and Tsuda*, 1997; *Guest et al.*, 2000; *Vincent and Alexander*, 2000]. Although the Jicamarca radar can only reach the lower edge of the stratosphere, the longer vertical wavelength of the tides suggests that they are less susceptible to diffusive damping and probably become increasingly important (relative to inertia-gravity waves) at higher levels.

[22] **Acknowledgments.** The help provided by the staff and engineers of Jicamarca Radio Observatory is gratefully acknowledged. The Observatory is operated by the Geophysical Institute of Peru, Ministry of Education, with support from the National Science Foundation of the United States. Chris Meyer and Elsayed Talaat assisted with the Hough mode solutions. The program used to read NCEP-NCAR reanalysis files was provided by Gilbert Compo. This research is supported by the Division of Atmospheric Sciences of the National Science Foundation through grants ATM-9709030 and ATM-9896193.

References

Bergman, J. W., and M. L. Salby, Equatorial wave activity generated by fluctuations in observed convection, *J. Atmos. Sci.*, *51*, 3791–3806, 1994.
Chapman, S., and R. S. Lindzen, *Atmospheric Tides*, D. Reidel, Norwell, Mass., 1970.
Dunkerton, T. J., The role of gravity waves in the quasi-biennial oscillation, *J. Geophys. Res.*, *102*, 26,053–26,076, 1997.
Forbes, J. M., Tidal and planetary waves, in *The Upper Mesosphere and Lower Thermosphere: A Review of Experiment and Theory, Geophys. Monogr. Ser.*, vol. 87, edited by R. M. Johnson and T. L. Killeen, AGU, Washington, D. C., 1995.
Fritts, D. C., and T. E. VanZandt, Effects of Doppler shifting on the frequency spectra of atmospheric gravity waves, *J. Geophys. Res.*, *92*, 9723–9732, 1987.
Fritts, D. C., and R. A. Vincent, Mesospheric momentum flux studies at Adelaide, Australia: Observations and a gravity wave/tidal interaction model, *J. Atmos. Sci.*, *44*, 605–619, 1987.
Fukao, S., S. Kato, S. Yokoi, R. M. Harper, R. F. Woodman, and W. E. Gordon, One full-day radar measurement of lower stratospheric winds over Jicamarca, *J. Atmos. Terr. Phys.*, *40*, 1331–1337, 1978.
Groves, G. V., Hough components of water vapour heating, *J. Atmos. Terr. Phys.*, *44*, 281–290, 1982.
Guest, F. M., M. J. Reeder, C. J. Marks, and D. J. Karoly, Inertia-gravity waves observed in the lower stratosphere over Macquarie Island, *J. Atmos. Sci.*, *57*, 737–752, 2000.
Hamilton, K., Latent heat as a possible forcing mechanism for atmospheric tides, *Mon. Weather Rev.*, *109*, 3–17, 1981.
Haurwitz, B., and A. D. Cowley, The diurnal and semidiurnal barometric oscillations: Global distribution and annual variation, *Pure Appl. Geophys.*, *103*, 193–222, 1973.
Hitchman, M. H., E. Kudeki, D. C. Fritts, J. M. Kugi, C. Fawcett, G. A. Postel, C.-Y. Yao, D. Ortland, D. Riggin, and V. L. Harvey, Mean winds in the tropical stratosphere and mesosphere during January 1993, March 1994, and August 1994, *J. Geophys. Res.*, *102*, 26,033–26,052, 1997.
Hsu, H.-H., and B. J. Hoskins, Tidal fluctuations as seen in ECMWF data, *Q. J. R. Meteorol. Soc.*, *115*, 247–264, 1989.
Kalnay, E., et al., The NCEP/NCAR 40-year reanalysis project, *Bull. Am. Meteorol. Soc.*, *77*, 437–471, 1996.
Kato, S., *Dynamics of the Upper Atmosphere*, D. Reidel, Norwell, Mass., 1980.
Lindzen, R. S., Internal gravity waves in atmospheres with realistic dissipation and temperature, part I, Mathematical development and propagation of waves into the thermosphere, *Geophys. Fluid Dyn.*, *1*, 303–355, 1970.
Lindzen, R. S., *Dynamics in Atmospheric Physics*, Cambridge Univ. Press, New York, 1990.
Maruyama, T., Upward transport of westerly momentum due to disturbances of the equatorial lower stratosphere in the period range of about 2 days: A Singapore data analysis for 1983–1993, *J. Meteorol. Soc. Jpn.*, *72*, 423–432, 1994.
McPhaden, M. J., Genesis and evolution of the 1997–98 El Niño, *Science*, *283*, 950–954, 1999.
Randal, D. L., T. H. V. Haar, M. A. Ringerud, G. L. Stephens, T. J. Greenwald, and C. L. Combs, A new global water vapor dataset, *Bull. Am. Meteorol. Soc.*, *77*, 1233–1246, 1996.
Riggin, D., D. C. Fritts, C. D. Fawcett, and E. Kudeki, Observations of inertia-gravity wave motions in the stratosphere over Jicamarca, Peru, *Geophys. Res. Lett.*, *22*, 3239–3242, 1995.
Riggin, D., D. C. Fritts, C. D. Fawcett, E. Kudeki, and M. H. Hitchman, Radar observations of gravity waves over Jicamarca, Peru during the CADRE campaign, *J. Geophys. Res.*, *102*, 26,263–26,281, 1997.
Salby, M. L., and R. R. Garcia, Transient response to localized episodic heating in the Tropics, part I, Excitation and short-term near field behavior, *J. Atmos. Sci.*, *44*, 458–498, 1987.
Sasi, M. N., L. Vijayan, V. Deepap, and B. V. Krishna Murthy, Estimation of equatorial wave momentum fluxes using MST radar winds observed at Gadanki (13.5°N, 79.2°E), *J. Atmos. Sol. Terr. Phys.*, *61*, 377–384, 1999.
Sassi, F., and R. R. Garcia, The role of equatorial waves forced by convection in the tropical semiannual oscillation, *J. Atmos. Sci.*, *54*, 1925–1942, 1997.
Sato, K., and T. J. Dunkerton, Estimates of momentum flux associated with equatorial Kelvin and gravity waves, *J. Geophys. Res.*, *102*, 26,247–26,261, 1997.
Shimizu, A., and T. Tsuda, Characteristics of Kelvin and gravity waves observed with radiosondes over Indonesia, *J. Geophys. Res.*, *102*, 26,159–26,171, 1997.
Tsuda, T., Y. Murayama, H. Wiryosumarto, S. W. B. Harijono, and S. Kato, Radiosonde observations of equatorial atmosphere dynamics over Indonesia, 2, Characteristics of gravity waves, *J. Geophys. Res.*, *99*, 10,507–10,516, 1994.
Tsuda, T., et al., A preliminary report on observations of equatorial atmosphere dynamics in Indonesia with radars and radiosondes, *J. Meteorol. Soc. Jpn.*, *73*, 393–406, 1995.
Tsuda, T., N. Nakamura, A. Shimizu, T. Yoshino, S. Woro, B. Harijono, T. Sribimawati, and H. Wiryosumarto, Observations of diurnal oscillations with a meteor wind radar and radiosondes in Indonesia, *J. Geophys. Res.*, *102*, 26,217–26,224, 1997.
VanZandt, T. E., A model for gravity wave spectra observed by Doppler sounding systems, *Radio Sci.*, *20*, 1323–1330, 1985.
Vincent, R. A., and M. J. Alexander, Gravity waves in the tropical lower stratosphere: An observational study of seasonal and interannual variability, *J. Geophys. Res.*, *105*, 17,971–17,982, 2000.
Wallace, J. M., and V. E. Kousky, Observational evidence of Kelvin waves in the tropical stratosphere, *J. Atmos. Sci.*, *24*, 900–907, 1968.
Wallace, J. M., and R. R. Tadd, Some further results concerning the vertical structure of atmospheric tidal motions within the lowest 30 kilometers, *Mon. Weather Rev.*, *102*, 795–803, 1974.
Warren, S. G., C. J. Hahn, J. London, R. M. Chevin, and R. L. Jenne, Global distribution of total cloud cover and cloud type over land, *NCAR Tech. Note NCAR/TN-273 + STR*, 229 pp., Natl. Cent. for Atmos. Res., Boulder, Colo., 1986.
Warren, S. G., C. J. Hahn, J. London, R. M. Chevin, and R. L. Jenne, Global distribution of total cloud cover and cloud type over the ocean, *NCAR Tech. Note NCAR/TN-317 + STR*, 170 pp., Natl. Cent. for Atmos. Res., Boulder, Colo., 1988.
Whiteman, C. D., and X. Bian, Solar semidiurnal tides in the troposphere: Detection by wind profilers, *Bull. Am. Meteorol. Soc.*, *77*, 529–542, 1996.
Williams, C. R., and S. K. Avery, Diurnal winds observed in the tropical troposphere using 50 MHz wind profilers, *J. Geophys. Res.*, *101*, 15,051–15,060, 1996.
Williams, C. R., S. K. Avery, J. R. McAfee, and K. S. Gage, Comparison of observed diurnal and semidiurnal tropospheric winds at Christmas Island with tidal theory, *Geophys. Res. Lett.*, *19*, 1471–1474, 1992.

Z. Feng and E. Kudeki, Department of Electrical and Computer Engineering, CSRL MC-229, University of Illinois, 1308 W. Main Street, Urbana, IL 61801, USA. (zfeng@uiuc.edu; erhan@deln.ece.uiuc.edu)

R. S. Lieberman and D. M. Riggin, Colorado Research Associates Division, NorthWest Research Associates, Inc., 3380 Mitchell Lane, Boulder, CO 80301, USA. (ruth@colorado-research.com; riggin@colorado-research.com)

M. F. Sarango, Instituto Geofisico del Perú, Jicamarca Radio Observatory, Apartado 3747, Lima 100, Peru. (sarango@jro.igp.gob.pe)

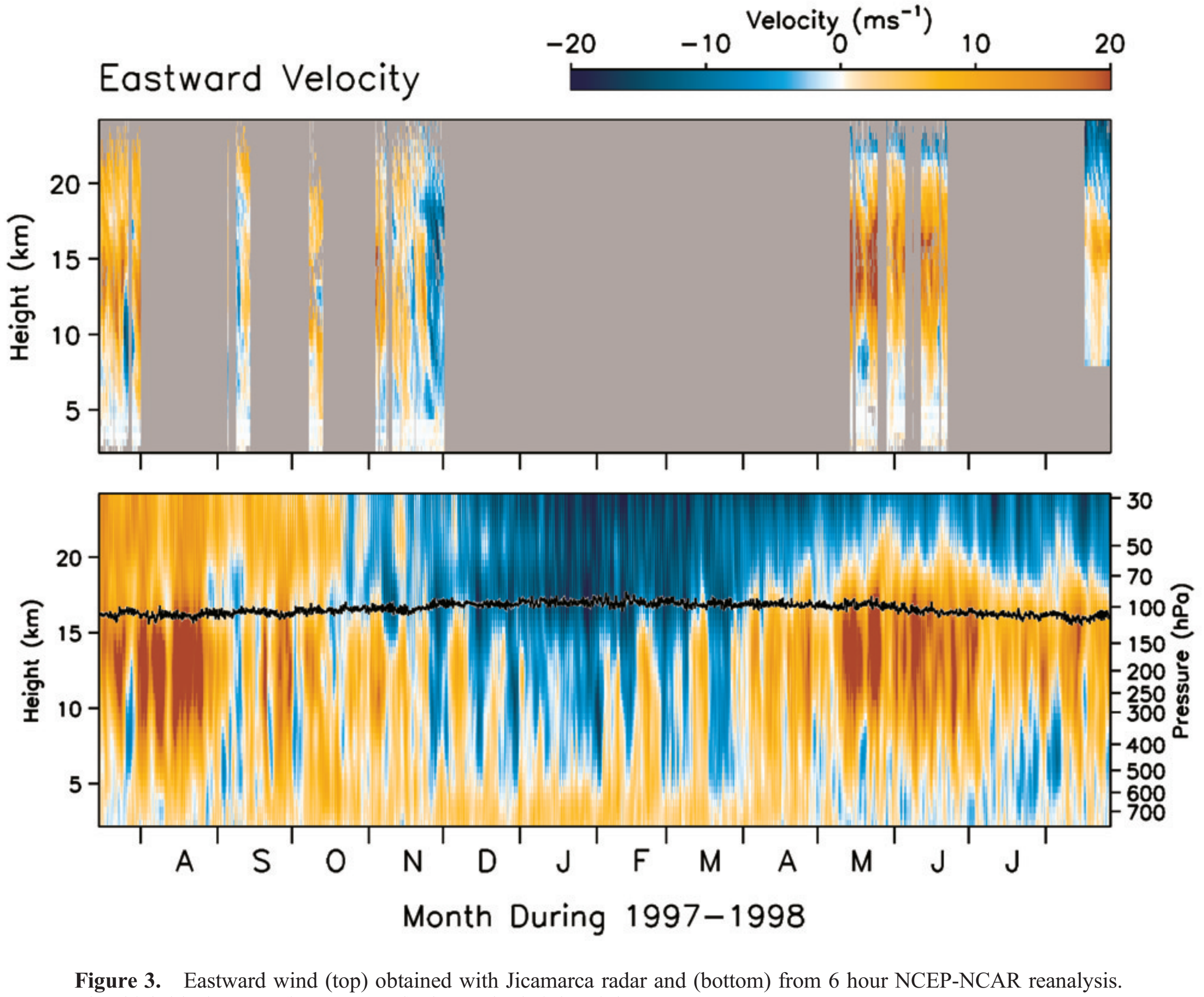

Figure 3. Eastward wind (top) obtained with Jicamarca radar and (bottom) from 6 hour NCEP-NCAR reanalysis. The thick black curve (bottom panel) shows the height of the tropopause.